
Associative Memories via Predictive Coding

Tommaso Salvatori¹, Yuhang Song^{1,3,*}, Yujian Hong¹, Lei Sha¹, Simon Frieder¹,
Zhenghua Xu², Rafal Bogacz³, Thomas Lukasiewicz¹

¹Department of Computer Science, University of Oxford, UK

²State Key Laboratory of Reliability and Intelligence of Electrical Equipment,
Hebei University of Technology, Tianjin, China

³MRC Brain Network Dynamics Unit, University of Oxford, UK

{tommaso.salvatori, yuhang.song, yujian.hong, lei.sha, frieder.simon, thomas.lukasiewicz}
@cs.ox.ac.uk, zhenghua.xu@hebut.edu.cn, rafal.bogacz@ndcn.ox.ac.uk

Abstract

Associative memories in the brain receive and store patterns of activity registered by the sensory neurons, and are able to retrieve them when necessary. Due to their importance in human intelligence, computational models of associative memories have been developed for several decades now. In this paper, we present a novel neural model for realizing associative memories, which is based on a hierarchical generative network that receives external stimuli via sensory neurons. It is trained using predictive coding, an error-based learning algorithm inspired by information processing in the cortex. To test the model’s capabilities, we perform multiple retrieval experiments from both corrupted and incomplete data points. In an extensive comparison, we show that this new model outperforms in retrieval accuracy and robustness popular associative memory models, such as autoencoders trained via backpropagation, and modern Hopfield networks. In particular, in completing partial data points, our model achieves remarkable results on natural image datasets, such as ImageNet, with a surprisingly high accuracy, even when only a tiny fraction of pixels of the original images is presented. Our model provides a plausible framework to study learning and retrieval of memories in the brain, as it closely mimics the behavior of the hippocampus as a memory index and generative model.

1 Introduction

Throughout our lives, we learn a huge number of associations between concepts: the taste of a particular food, the meaning of a gesture, or to stop when we see a red light. Every time we acquire new information of this kind, it gets stored in our long-term memory, situated in distributed networks of brain areas [1]. In particular, visual memories are stored in a hierarchical network of visual and associative areas [2]. These regions learn progressively more abstract representations of visual stimuli, so they participate in both perception and memory as each area memorizes relationships present in their inputs [3]. Accordingly, early visual areas learn common regularities present in the stimuli [4], while at the top of this hierarchy, associative areas (such as hippocampus, entorhinal cortex, and perirhinal cortex) store the relationships between extracted features, which encode an entire stimulus or episode [5]. The memory system of the brain is able to both recall complex memories [1, 6], and use them to generate predictions to guide behavior [7]. Learning in these associative memories shapes our understanding of the world around us and builds the foundations of human intelligence.

Building models that are able to store and retrieve information has been an important direction of research in artificial intelligence. Particularly, such models include (auto)associative memories (AMs), which allow for the storage of data points and their contents-based retrieval, i.e., for retrieving a stored

*Corresponding author

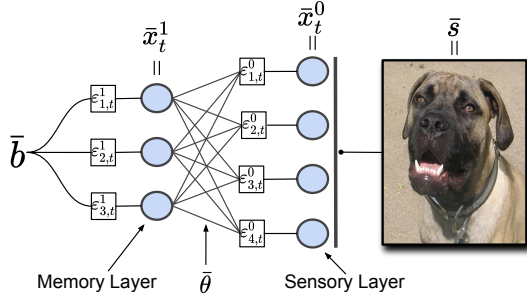


Figure 1: Generative PCN with two layers. Each line linking neurons denotes a pair of connections (excitatory in the left direction, and inhibitory in the right direction). At $t = 0$, the value nodes of the output layer are fixed to the vector representing the pixels of the figure. Then, during the learning phase, both weight parameters and value nodes are updated.

data point s from a corrupted or a partial variant of s . One way to realize AMs is to store data points as attractors, so that they can be easily recovered via an energy minimization process when presenting their corrupted variants [8, 9]. Existing AMs include Hopfield networks [8] and modern Hopfield networks (MHNs) [10]. The latter are one-shot learners, which are able to store exponentially many memories, and to perfectly retrieve them. However, the retrieval process often fails when dealing with complex data, such as natural images. Recent works have shown that overparametrized autoencoders (AEs) are excellent AMs as well. Particularly, when training an AE to generate a specific point s when s itself is presented as an input, it gets stored as an attractor [11].

In this work, we present a novel AM model that is based on an energy-based generative approach. This AM model differs from Hopfield networks, as it is trained using predictive coding (PC), which is a biologically plausible learning algorithm inspired by learning in the visual cortex [4]. The idea that PC may naturally be related to AMs is inspired by recent works showing that the generative neural architecture that connects the hippocampus to the neocortex is based on an error-driven learning algorithm, which can be interpreted with a PC framework [6, 12]. From a machine learning perspective, predictive coding networks (PCNs) are able to perform both supervised and unsupervised tasks with a high accuracy [4, 13], and are completely equivalent to backpropagation when trained with a specific algorithm [14–16]. We show that the new AM model is not only interesting from a neuroscience perspective, but it also outperforms popular AM models when it comes to the storage and retrieval of complex data points. Our results can be briefly summarized as follows:

- We define generative PCNs and empirically show that they store training data points as attractors of their dynamics by demonstrating that they can restore original data points from corrupted versions. In an extensive comparison of the new AM model against standard AEs, the new model considerably outperforms AEs (in storage capacity, retrieval accuracy, and robustness) when tested on neural networks of the same size.
- The reconstruction of incomplete data points is a challenging task for AMs. Our model naturally solves the task of reconstructing complex and colored images with a surprisingly high accuracy. We also test our model on ImageNet, perfectly reconstructing single pictures even after removing all but 1/8 of the original image. We then show that, to increase the overall capacity and retrieval robustness of the model, it suffices to add additional layers. We also compare our model against MHNs, showing that it significantly outperforms them in the aforementioned tasks.

2 Generative predictive coding networks

We now briefly recall predictive coding networks (PCNs), and we introduce generative PCNs, which are the underlying neural model for the novel AMs introduced in the subsequent section.

Deep neural networks have a multi-layer structure, where each layer is formed by a vector of neurons [17]. While in standard deep learning the goal is to minimize the error on a specific layer, PC defines an error in every layer of the network, minimized by gradient descent on a global energy function [4]. Particularly, let M be a PCN with $L - 1$ fully connected layers of dimension n , followed by a fully connected layer of dimension d . We call the d -dimensional layer *sensory* layer (indexed as layer 0), which biologically corresponds to sensory neurons (see Fig. 1). We call the most internal layer (layer L) *memory*, which is equipped with an n -dimensional memory vector b . Every layer l contains value nodes $x_{i,t}^l$, and every pair of consecutive layers is connected via weight matrices $\bar{\theta}^l$, which represent the synaptic weights between neurons of different layers. The value nodes, the

Algorithm 1: Learning to generate \bar{s} with IL

Require: \bar{x}_0 is fixed to \bar{s} .

- 1: **for** $t = 0$ to T **do**
 - 2: **for** each neuron i in each level l **do**
 - 3: update $x_{i,t}^l$ to minimize E_t via Eq.(3)
 - 4: **end for**
 - 5: **end for;**
 - 6: update each $\theta_{i,j}^{l+1}$ and b_i to minimize E_t via Eqs. (4) and (5).
-

weight matrices, and the memory vector are all trainable parameters of the model. The signal passed from layer $l + 1$ to layer l , called prediction $\bar{\mu}_t^l$, is computed as follows:

$$\mu_{i,t}^l = \begin{cases} \sum_{j=1}^{n^{l+1}} \theta_{i,j}^{l+1} f(x_{j,t}^{l+1}) & \text{if } 0 \leq l < L \\ b & \text{if } l = L, \end{cases} \quad (1)$$

where f is a non-linear activation function. To conclude, the difference between the value \bar{x}_t^l and their predictions $\bar{\mu}_t^l$ is the *error* $\varepsilon_{i,t}^l = x_{i,t}^l - \mu_{i,t}^l$. We now describe how PCNs are trained. To do this, we explain one iteration of a training algorithm, called *inference learning (IL)*, that is divided into an inference phase and a weight update phase.

Inference: Only the value nodes of the network are updated, while both the weight parameters and the memory vector are fixed. Particularly, the value nodes are modified via gradient descent to minimize the global error of the network, expressed by the following energy function E_t :

$$E_t = \frac{1}{2} \sum_{i,l} (\varepsilon_{i,t}^l)^2. \quad (2)$$

Assume that we train a generative PCN on a training point $\bar{s} \in \mathbb{R}^d$. To do this, the value nodes of the sensory layer are fixed to the training point \bar{s} , and are never updated. Thus, the error on every neuron of the sensory layer is equal to $\varepsilon_{i,t}^0 = s_i - \mu_{i,t}^0$. The process of minimizing E_t by modifying all $x_{i,t}^l$ leads to the following changes in the value nodes:

$$\Delta x_{i,t}^l = \begin{cases} \gamma \cdot (-\varepsilon_{i,t}^l + f'(x_{i,t}^l) \sum_{k=1}^{n^{l-1}} \varepsilon_{k,t}^{l-1} \theta_{k,i,t}^l) & \text{if } 0 < l \leq L \\ 0 & \text{if } l = 0, \end{cases} \quad (3)$$

where γ is the *integration step*, which is a constant determining by how much the activity changes in each iteration. The computations in Eqs. (1) and (3) are biologically plausible, as they have a neural implementation that can be realized in a network with value nodes $x_{i,t}^l$ and error nodes $\varepsilon_{i,t}^l$ [4], as shown in Fig. 1. The inference phase works as follows: starting from a given configuration of the value nodes \bar{x}_0 , inference continuously updates the value nodes according to Eq. (3) until it has converged. We call the configuration of the value nodes at convergence \bar{x}_T , where T is the number of steps needed to reach convergence (in practice, it is a fixed large number).

Weight Update: When the value nodes of the sensory layer are fixed to an input signal \bar{s} , inference may not be sufficient to reduce the total energy to zero. Hence, to further decrease the total error, a single *weight update* is performed: both the weight matrices and the memory vector are updated by gradient descent to minimize the same objective function E_t , and behave according to the following equations, where α is the learning rate. Particularly, the derived update rule is the following:

$$\Delta \theta_{i,j}^{l+1} = -\alpha \cdot \partial E_T / \partial \theta_{i,j}^{l+1} = \alpha \cdot \varepsilon_{i,T}^l f(x_{j,T}^{l+1}), \quad (4)$$

$$\Delta b_i = -\alpha \cdot \partial E_T / \partial b_i = -\alpha \varepsilon_{i,T}^L. \quad (5)$$

The phases of inference and weight update are iterated until the total energy E_t reaches a minimum. This algorithm learns a dataset by using only local computations, which minimize the same energy function. Fig. 1 gives a graphical representation of generative PCNs, while the pseudocode is shown in Alg. 1. Detailed derivations of Eqs. (3) and (5) are in the supplementary material (and in [13]).

3 Predictive coding for associative memories

So far, we have shown how PCNs can perform generative tasks. We now show how generative PCNs can be used as associative memories, i.e., how the model stores the data points that it is trained on, and how these data points can be retrieved when presenting corrupted versions to the network, returning

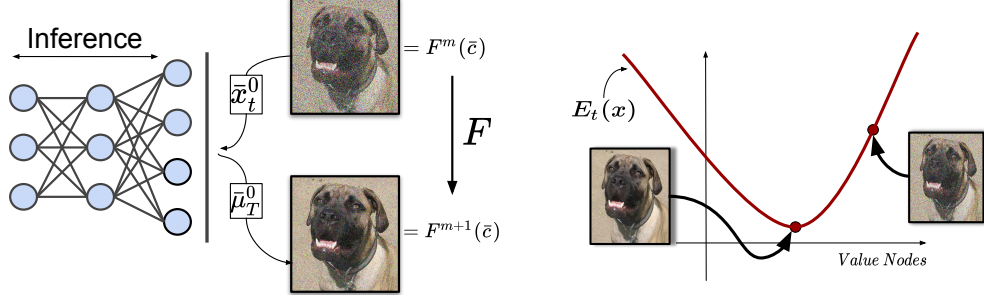


Figure 2: Left: Representation of the function F , used to retrieve stored images. It can be decomposed into three steps: (1) The value nodes of the sensory layer are fixed to the pixels of the corrupted image $F^m(\bar{c})$. (2) Inference runs for T operations (until convergence). (3) We set $F^{m+1}(\bar{c})$ to the prediction of the sensory layer $\bar{\mu}_T^0$. Note that the weight parameters are never updated during the above steps. We have omitted the error nodes for simplicity. Right: Representation of an AM, where an image \bar{s} (photo of a dog) is stored as an attractor of the dynamics. A corrupted image that lies in a specific neighborhood of \bar{s} converges to it when minimizing the total energy via running inference.

the most similar stored data point. Let \bar{s} be a training data point, and M be the PCN considered above, already trained until convergence to generate \bar{s} . Moreover, assume that M makes the total energy converge to *zero* at iteration T . At this point, the energy function defined on the value nodes has a local minimum \bar{x} in which the value nodes of the sensory layer are equal to the entries of \bar{s} . Note that \bar{x} is actually an attractor of the dynamics of E_t : when given a configuration that is not a local minimum, inference will update the value nodes until the total energy reaches a minimum. If this configuration lies in a specific neighborhood of \bar{x} , inference will converge to \bar{x} . So, given a dataset, we obtain an AM of the dataset if all the training points are stored in the above way as attractors.

The above can be used to retrieve stored data points \bar{s} : given a corrupted version $\bar{c} \in \mathbb{R}^d$ of \bar{s} , one can retrieve \bar{s} as follows. First, we set the value nodes of the sensory layer to the corrupted points, i.e., $\bar{x}_t^0 = \bar{c}$ for the whole process. Then, we run inference until convergence and save the prediction $\bar{\mu}_T^0$ of the sensory layer. If the original data point was stored as an attractor, we expect the prediction $\bar{\mu}_T^0$ to be a less corrupted version of it. Let $F: \mathbb{R}^d \rightarrow \mathbb{R}^d$ be the function that sends \bar{c} to $\bar{\mu}_T^0$ just described, and summarized in Fig. 2. Many iterations of this function allow to retrieve the stored data point. Hence, summarizing the above, training points are stored in the memory vector \bar{b}_T and the weight parameters, and what the algorithm does to retrieve them is simply the inference phase of PCNs. Since visual memories are stored in hierarchical networks of brain areas, PC could be a highly plausible algorithm to better understand how memory and prediction work in the brain.

To experimentally show that generative PCNs are AMs, we trained a 2-layer network with ReLU non-linearity on a subset of 100 images of Tiny ImageNet and CIFAR10. After training, we presented the model with a corrupted variant (by adding Gaussian noise) of the training set. We then used the PCNs to reconstruct the original images from the corrupted ones. The experimental results confirm that the model is able to retrieve the original image, given a corrupted one. The obtained reconstructions for the Tiny Imagenet dataset (the most complex one, as each data point consists of $3 \times 64 \times 64$ pixels) are shown in Fig. 4. We now provide a more comprehensive analysis, which studies the capacity of generative PCNs when changing the number of data points and parameters.

Experiments: We trained 2-layer PCNs with ReLU non-linearity and hidden dimension $n \in \{512, 1024, 2048\}$ on subsets of the aforementioned datasets of cardinality $N = \{100, 250, 500, 1000\}$. Every model is trained until convergence, and all the images are retrieved as described in Section 3. To provide a numerical evaluation, an image is considered recovered when the mean squared error between the original image and the recovered image is less than 0.005.

To compare our results against a standard baseline, we also trained 3-layer autoencoders (AEs) with the same hidden dimension on the same task, and compared the results. Note that the number of parameters of a 2-layer PCN is smaller than the one of a 3-layer AE with the same hidden dimension. This follows, as the additional layer (input layer, not needed in generative PCNs) almost doubles the number of parameters in some cases. Further details about the experiments and used hyperparameters are given in the supplementary material.

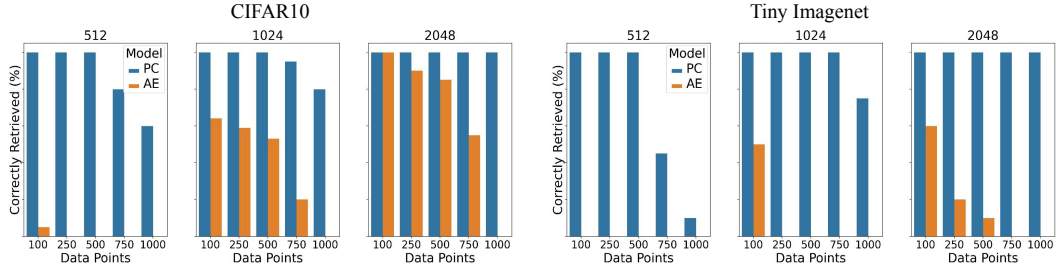


Figure 3: Percentage of correctly retrieved images by 2-layer generative PCNs (PC) and 3-layer autoencoders (AE) with hidden-layer dimensions of 512, 1024, and 2048, when presented with a corrupted image with Gaussian noise of variance 0.2 of CIFAR10 and of Tiny ImageNet.

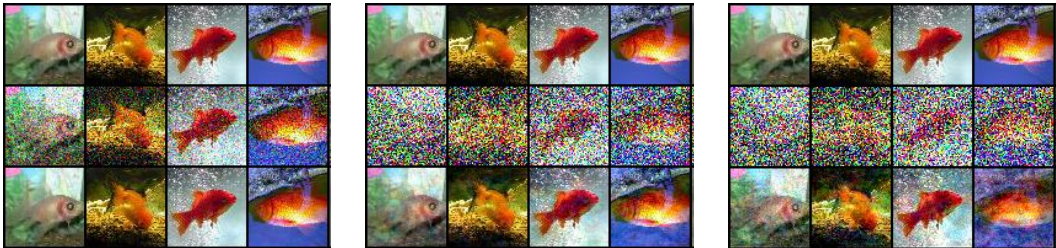


Figure 4: Reconstructions of 64×64 Tiny ImageNet images with noise levels 0.2, 0.7, and 0.9, respectively (original, noisy, and reconstructed image in first, second, and third row, respectively).

Results: The analysis shows that our model is able to store and retrieve data points even when the network is not overparametrized (see Fig. 3). AEs trained with BP did not perform well: AEs with less than 1024 hidden neurons always failed to restore even a single data point on the Tiny ImageNet dataset, and very few on other ones. The performance of AEs with 2048 hidden neurons were always worse than PCNs with 512 hidden neurons. This shows that overparametrization is essential for AEs to perform AM tasks, and that our proposed method offers a much more network-efficient alternative.

In terms of capacity, 2-layer PCNs with 512 hidden neurons correctly store datasets of 250 images of both CIFAR10 and Tiny ImageNet, and networks with 2048 hidden neurons always store and retrieve all the presented datasets. As typical for AMs, small models trained on large datasets fail to store data points, as the space of parameters is not large enough to store each data point as an independent attractor. Our model is no different: PCNs with 512 hidden units are able to store almost 500 Tiny ImageNet images when trained on datasets of that size, but fail to store more than 200 when trained on larger ones.

4 Retrieval from partial data points

So far, we have shown how the proposed generative model can be used to retrieve stored data points when presented with corrupted variants. We now tackle the different task of retrieving data points when presented with partial ones. Let \bar{s} be the stored data point, and assume that a fraction of pixels of \bar{s} are accessible, and the goal is to retrieve the remaining ones. Let \bar{s}' be the vector of the same dimension of \bar{s} , where a fraction of pixels are equal to the ones of the stored data point, and assume that the position of the pixels that are equal to the ones of \bar{s} is known. We now show how to retrieve the complete data point by using the same network M , trained as already shown in Section 3.

Let M be a PCN trained to generate \bar{s} . Then, given the partial version of the original data point \bar{s}' , it is possible to retrieve the full data point using M as follows: first, we only fix the value nodes of the sensory layer \bar{x}_t^0 to the entries of the partial data point \bar{s}' that we know are equal to the ones of the stored data point, leaving the rest free to be updated. Then, we run inference on the whole network until convergence. At this point, we expect the value nodes \bar{x}_T^0 to have converged to the entries of the original data point, stored as an attractor. A graphical representation of the above mechanism is described in Fig. 5. To show the capabilities of this network, we have performed multiple experiments on the Tiny ImageNet and ImageNet datasets, and compared against existing models in the literature.

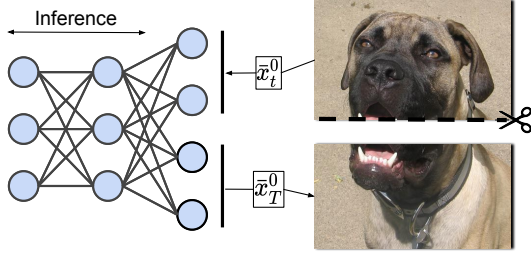


Figure 5: Algorithm used to retrieve a stored data point from a fraction of it: (1) The value nodes of the sensory layer that correspond to the available entries of \bar{s} are fixed to the respective values. (2) Inference runs for T operations (until convergence). (3) We set our prediction to be equal to the value nodes of the sensory layer \bar{x}_T^0 . The weight parameters are never updated during the above steps. The error nodes are omitted for simplicity.

Algorithm 2: Retrieving \bar{s} given a non-corrupted fraction \bar{s}'

Require: if s'_i a correct entry of the original memory, then $x_{i,t}^0$ is fixed to s'_i .

- 1: **for** $t = 1$ to T **do**
 - 2: **for** each neuron i in each level l **do**
 - 3: update $x_{i,t}^l$ to minimize E_t
 - 4: **end for**
 - 5: **end for;**
 - 6: **return** \bar{x}_T^0 .
-

We now start by providing visual evidence on the effectiveness of this method. Note that the geometry of the mask does not influence the final performance, as our model simply memorizes single pixels.

Experiments: We trained two networks with hidden dimensions of 1024 and 2048, to generate 50 images of the first class of Tiny ImageNet (corresponding to goldfishes), and a network of 8192 hidden neurons to reconstruct 25 ImageNet images. Then, we used inference as explained to retrieve the original images. We considered an image to be correctly reconstructed when the error between the original and the retrieved image was smaller than 0.001. Furthermore, we plotted the partial images together with their reconstructions, for a visual check. Note that we used the thresholds that provided the fairest comparison: the denoising experiments fail to have a perfect retrieval, despite the fact that most of the images look visually good. Hence, we determined the threshold to be equal to 0.005. Then, with the same threshold for the retrieval of partial images, our method always successfully retrieved all the images, and so we opted for a smaller threshold, which was more informative.

Results: On Tiny ImageNet, a generative PCN with 1024 hidden neurons managed to reconstruct all the images when presented with 1/8 of the original image, and more than half for the smallest fraction considered, 1/16. The network with 2048 neurons also failed to reconstruct all the images when presented with 1/16 of the original image. However, even when presented with a portion as small as 1/16 of the original image, the reconstruction was clear, although not perfect and hence now above our threshold. This result is shown in Fig. 6 (left).

Surprisingly, generative PCNs trained on ImageNet correctly stored all the presented training images, and correctly reconstructed them with no visible error. This shows that PCNs can be used to store high-dimensional and high-quality images in practical setups, which can be retrieved using only a low-dimensional key, formed by a fraction of the original image. Particularly, Fig. 6 (right) shows the perfect reconstruction obtained on ImageNet when the network is presented with only 1/8 of the original image. Further experiments on ImageNet are shown in the supplementary material, where we present multiple high-quality reconstructions.

5 More training data points and/or deeper PCNs

In the above experiments, a shallow architecture is able to store 100 natural images from Tiny ImageNet, and to reconstruct them with no visible error when provided with 1/8 of the original images. We now study how this changes when either the cardinality of the dataset is increased, or the number of provided pixels during reconstruction is updated. To study this, we have trained two models with $n = \{1024, 2048\}$ hidden units on subsets of Tiny ImageNet of cardinality $N = \{50, 100, 250, 500\}$, and reconstructed images with only $p = \{1/2, 1/4, 1/8, 1/16\}$ of the original images. According to our visualization experiments, we have noted that an image has no visible reconstruction noise when

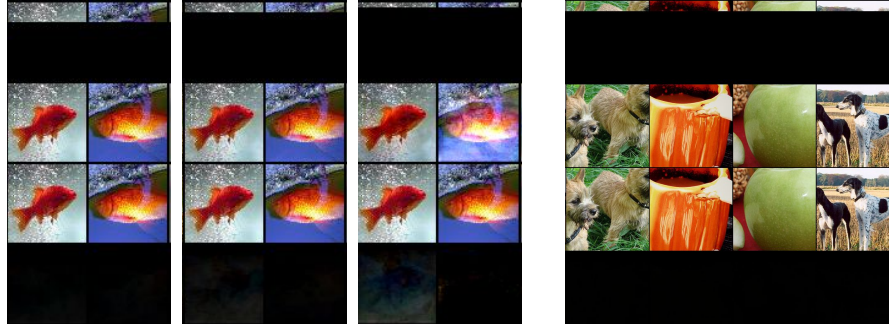


Figure 6: Partial images and their reconstructions (from top to bottom: partial image, reconstructed image, original image, and reconstruction error (difference between original and reconstruction)). Left: 64×64 Tiny ImageNet images presented with $1/4$, $1/8$, and $1/16$ of the original image, respectively, using a network of 1024 hidden neurons. Right: 224×224 ImageNet images presented with $1/8$ of the original image, using a network with 8196 hidden neurons.

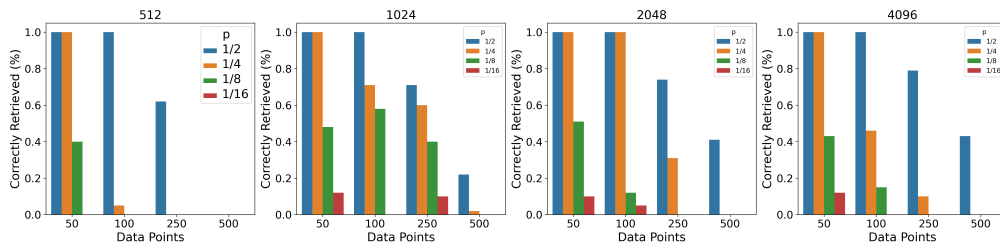


Figure 7: Percentage of perfectly retrieved images given different fractions of the original images for PCNs with 512, 1024, 2048, and 4096 hidden neurons trained on datasets of different sizes. Note that here we count as retrieved only images with non-visible errors. Most of the images that are not considered retrieved in this plot, were correctly retrieved, but only slightly noisy.

the error between the original image and the reconstruction is less than 0.001. Hence, we consider an image to be correctly retrieved if the reconstruction error is below this threshold.

Results: Every network with 50 stored memories was able to perfectly reconstruct the original image when provided with $1/4$ of it, and about half when provided with only $1/8$. However, this changes when increasing the training set, as no network trained on more than 50 images was able to correctly reconstruct an image when provided with $1/16$ of it, besides a few cases. In terms of capacity, the more images we train on, the harder the reconstruction becomes: no training image was correctly retrieved when training on $N = 500$ images when provided with a fraction smaller than $1/2$ of the original image, regardless of the width of the network. A summary of these results is given in Fig. 7.

These experiments show the limits of shallow generative PCNs on both reconstruction capabilities and capacity. As expected and common in standard AM experiments, increasing the number of training points and reducing the number of available information for reconstruction hurts the performance. We now show how increasing the number of layers solves this capacity problem.

Deep generative PCNs. We now test how increasing the depth of generative PCNs increases their capacity. We then compare the results against overparametrized AEs. Particularly, we trained generative PCNs with $n = \{1024, 2048\}$ hidden neurons, depth $L = \{3, 5, 7, 10\}$ on $N = 500$ images of Tiny ImageNet. Furthermore, we reconstructed the stored images using a fraction of $p = \{1/2, 1/4\}$ of the original images. To further compare against state-of-the-art AEs, we trained equivalent AEs, which is the best-performing one according to [11]. Also, all the hyperparameters used for training are the ones reported by the authors. To make the comparison completely fair, we also assume that the correct pixels of the incomplete images are known when testing the AE. Particularly, we fixed these pixels at every iteration of the reconstruction process of the AEs. As above, we consider an image to be correctly retrieved if the reconstruction error is less than 0.001.

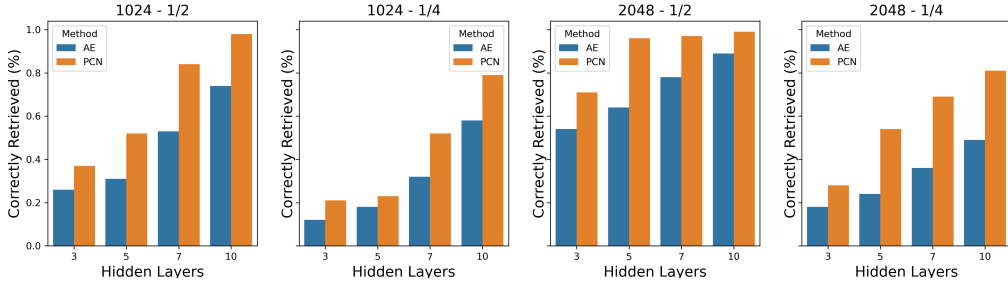


Figure 8: Percentage of correctly retrieved images as a function of the number of hidden layers, for both AEs and generative PCNs, on a dataset of 500 images. We used networks with $n = \{1024, 2048\}$ hidden neurons, and the images are taken from Tiny ImageNet.

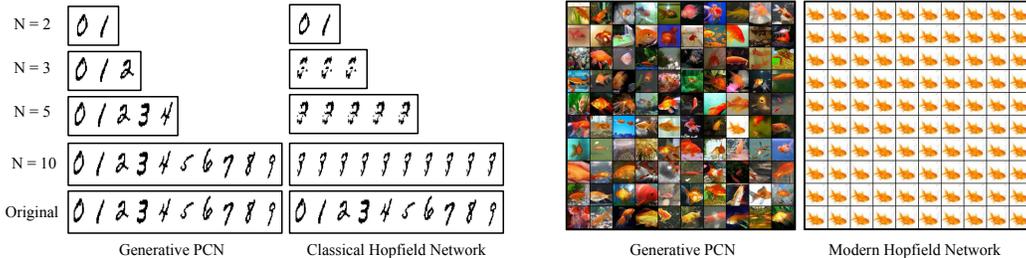


Figure 9: Left: Recovery of 2, 3, 5, and 10 MNIST images using a generative PCN and classical Hopfield networks [8] when presented with 1/2 of the original image as a key. As shown, Hopfield networks only recovered the original images when $N = 2$, but otherwise always failed to retrieve them when trained on more than two images. Right: Reconstruction of 100 Tiny ImageNet images when provided with 1/2 of the original image, using a generative PCN and a MHN with $\beta = 2$.

Results: The results confirm the hypothesis: the deeper the network, the higher the capacity. Particularly, a 10-layer network was able to reconstruct more than 98% (against the 72% of the AE) of the images when providing half of the original pixels, and 74% (against the 48% of the AE) of the images when providing 1/4 of the pixels. This shows that our model clearly outperforms state-of-the-art AEs in image reconstruction, even in the overparametrized regime. Fig. 8 summarizes these results.

6 Comparison with Hopfield networks

In this section, we compare against the most popular AM models, namely, classical and modern Hopfield networks (MHNs) [8, 10]. Despite their popularity, both types of Hopfield networks fail to retrieve complex data such as natural images. We now show that the retrieval process of our model is significantly better, as it always converges to a plausible solution, even when provided with a tiny amount of information, or a large amount of corruption.

Classical Hopfield networks. We now compare against classical Hopfield networks [8]. We have trained a Hopfield network on $N = \{2, 3, 5, 10\}$ images of the MNIST dataset, and converted every grey-scale pixel to either 0 or 1, as Hopfield networks only work on binary data. However, this model was able to retrieve the original images when presented with 1/2 only when $N = 2$. To test generative PCNs on the same task, we used a small network with one hidden layer and 32 hidden neurons. Our model was always able to retrieve the original images. Visual results of this experiments are shown in Fig. 9 (left).

Modern Hopfield networks. We trained an MHN to memorize 50/100/250/500 CIFAR10 images, and then performed three different experiments. In the first two, we tried to reconstruct the original

N	$p = 1/2$	$p = 1/4$	$\eta = 0.2$
50	5	4	4
100	4	3	3
250	1	1	9
500	1	1	3

Table 1: Number of correctly retrieved images on different tasks by a MHN trained on fractions of CIFAR10.

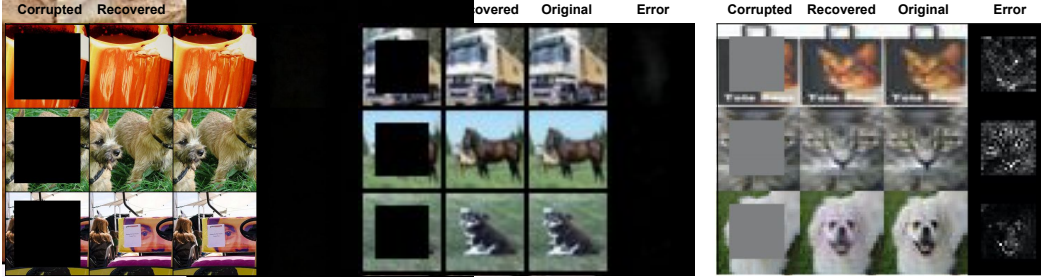


Figure 10: Left: Our reconstruction on 25 ImageNet 224×224 images and a network with 8192 hidden neurons. Centre: Our reconstruction using a generative PCN with 1024 hidden neurons on CIFAR10 32×32 images. Right: Reconstruction of a DANN on the same dataset (taken from [18]).

memories when providing $1/2$ and $1/4$ of the original image as a key. Then, we corrupted the original images by adding Gaussian noise. Despite the high capacity, MHNs do not perform well in image retrieval. Particularly, they were able to retrieve at most 9 images when presented with a corrupted image, and at most 5 when presented with an incomplete one. The results of the experiment are given in Table 1. In Fig. 9 (right), we provide a visual comparison between our method and MHNs, showing that they are only able to retrieve one image when trained on complex images taken from the Tiny Imagenet dataset. Further details about the experiments are given in the supplementary material.

Deep associative neural networks. To improve their performance, MHNs have been augmented with a convolutional multilayer structure for unsupervised feature detection [18]. The resulting architecture, called *deep associative neural network* (DANN), is able to perform both AM and classification tasks. We now compare the image reconstruction experiments performed in [18] with the ones performed by our generative PCN. We replicate the experiment proposed, which consists in presenting the network an partial image of the CIFAR10 dataset, where a squared patch covers the centre of each image. Note that this is not a completely fair comparison, as (1) DANNs merge AM with convolutions and unsupervised feature detection layers, and (2) it is trained on the whole dataset. Hence, comparing it against a pure AM model such as ours may be unfair. However, we believe that presenting comparisons against models that perform AM tasks such as DANNs is still interesting in understanding how our model compares against existing ones in the literature.

We first ran the same experiment on CIFAR10 as in [18]. Particularly, we used 250 images. The comparison is given in Fig. 10. Unlike the image in [18], our reconstruction shows no visible error. Furthermore, we replicated the experiment using 50 images of ImageNet, and showed that our model is again able to provide perfect reconstructions of the original images.

7 Biological relevance

The model described in this paper is closely related with theories of functioning of the memory system in the brain. It is typically assumed that memories are stored in a network of cortical areas organized hierarchically, where sensory information is processed and encoded by several neo-cortical regions, and then it is integrated across modalities in the hippocampus [2, 5]. It has been recently proposed that this hippocampo-neocortical system can be viewed as a PCN [6] similar to the one in this paper. In particular, Barron et al. [6] proposed that the hippocampus could be viewed as a top layer in the hierarchical PCN (which would correspond to the memory layer L in our model), while neo-cortical areas would correspond to lower layers in the network. A contribution of our paper is to implement this idea and demonstrate in simulations that PCNs, which were only theoretically proposed to act as a memory system [6], can actually work and effectively store and retrieve memories.

The mechanisms of learning and retrieval proposed in the PC account of the brain memory system in [6] closely resemble those occurring in our model. Barron et al. proposed that during learning, the generative model of the hippocampus is updated until the hippocampal predictions correct the prediction errors by suppressing neo-cortical activity [6]. The training phase of our generative model closely resembles this framework, as it also accumulates prediction errors from the sensory neurons to the hidden layers and memory vector, while a continuous update of the value nodes corrects the errors in the sensory neurons. Then, the parameters of our generative model are updated until its predictions reach low/zero error in the sensory neurons. Learning in PCNs relies on local Hebbian rules, i.e., the

weights between co-active neurons are increased, and such form of synaptic plasticity has been first demonstrated experimentally in the hippocampus [19]. It has been further suggested that during the reconstructions of past memories, the hippocampus sends descending input to the neocortical neurons to reinstate activity patterns that recapitulate previous sensory experience [6]. In the reconstruction phase of our generative model, the memory vector provides descending inputs to the sensory neurons, to generate patterns that recall previous sensory experience, e.g., stored data points.

Our model captures certain high-level features of the brain memory system, but many details of the model will have to be refined to describe biological memory networks. Barron et al. [6] reviewed in detail how the architecture of a PC model could be related to the known anatomy of neo-cortical memory areas, and how different populations of neurons and connections in the model could be mapped on known groups of neurons and projections in the neo-cortex. Interesting future work is to extend the top layer of our memory network to include key features of the hippocampus, i.e., recurrent connections, known to exist in the subfield CA3, as well as an additional population of neurons in dentate gyrus and CA1, which have been proposed to play specific roles in learning new memories [20]. It is also interesting to investigate if our model can reproduce experimental data on how the hippocampus drives the reinstatement of stored patterns in the neo-cortex during retrieval [21, 22].

8 Related work

Predictive coding [4] and AM models [8, 23] have rarely been related in the literature to date. However, they share multiple similarities, the main of which is that both are energy-based models that update their parameters using local information.

Associative memories (AMs). In computer science, AMs date back to 1961, with the introduction of the *learn matrix* [24], a hardware implementation of hetero-associative memories using ferromagnetic properties. However, the milestones of the field are Hopfield networks, presented in the early eighties in their discrete [8] and continuous [23] version. Recently, AMs have increasingly gained popularity. Particularly, a 2-layer version of Hopfield networks with polynomial activations has been shown to have a surprisingly high capacity [10], which can be increased even more with exponential activations [25, 26]. The recent focus of the machine learning community on AM models, however, does not lie in applying them directly to solve practical hetero-associative memory tasks. On the contrary, it has been shown that modern architectures are implicitly AMs. Examples of these are standard deep neural networks [27, 11] and transformers [28]. Hence, there is a growing belief that understanding AM models will help the understanding and improvements of deep learning [29, 27, 30, 31]. In fact, different classification models perform well when augmented with AM capabilities. DANNs [18], e.g., use deep belief networks to filter information, while [32] improves over standard convolutional models by adding an external memory that memorizes associations among images.

Predictive coding (PC). This framework includes both a biologically plausible neural architecture and a learning algorithm [4] developed to emulate learning in the visual cortex. Particularly, PC allows to describe multiple phenomena happening in the brain, using a single framework, such as free-energy minimization with local computations [33–36]. From the more practical point of view, PC can be used to train high-performing neural architectures [13, 37, 38], as it has been shown that it can exactly replicate the weight update of BP [14–16].

9 Conclusion

In this paper, we have shown that predictive coding (which was originally designed to simulate learning in the visual cortex) naturally implements associative memories that have a high capacity and a high retrieval accuracy and robustness, and that can be expressed using small and simple fully connected neural architectures. We have shown this empirically in a large number of experiments. Particularly, we have performed denoising and image reconstruction tasks, comparing against standard autoencoders. Furthermore, we have shown that this model is able to reconstruct with no visible error natural high-resolution images of the ImageNet dataset, when provided with a tiny fraction of them. Overall, this work strengthens the connection between the machine learning and the neuroscience community. It underlines the importance of predictive coding in both areas, both as a highly plausible algorithm to better understand how memory and prediction work in the brain, and as an approach to solve corresponding problems in machine learning and artificial intelligence.

Acknowledgments and Disclosure of Funding

This work was supported by the Alan Turing Institute under the EPSRC grant EP/N510129/1 and by the AXA Research Fund. This work was also supported by the China Scholarship Council under the State Scholarship Fund, by the UK Medical Research Council under the grant MC_UU_00003/1, by the National Natural Science Foundation of China under the grant 61906063, by the Natural Science Foundation of Hebei Province, China, under the grant F2021202064, by the Natural Science Foundation of Tianjin City, China, under the grant 19JCQNJC00400, and by the “100 Talents Plan” of Hebei Province, China, under the grant E2019050017.

References

- [1] L. Squire and S. Zola-Morgan, “The medial temporal lobe memory system,” *Science*, vol. 253, no. 5026, 1991.
- [2] D. J. Felleman and D. C. Van Essen, “Distributed hierarchical processing in the primate cerebral cortex,” *Cerebral Cortex*, vol. 1, no. 1, pp. 1–47, 1991.
- [3] E. A. Murray, T. J. Bussey, and L. M. Saksida, “Visual perception and memory: A new view of medial temporal lobe function in primates and rodents,” *Annual Reviews Neuroscience*, vol. 30, pp. 99–122, 2007.
- [4] R. P. Rao and D. H. Ballard, “Predictive coding in the visual cortex: A functional interpretation of some extra-classical receptive-field effects,” *Nature Neuroscience*, vol. 2, no. 1, pp. 79–87, 1999.
- [5] J. McClelland, B. McNaughton, and R. O’Reilly, “Why there are complementary learning systems in the hippocampus and neocortex: Insights from the successes and failures of connectionist models of learning and memory,” *Psychological Review*, vol. 102, pp. 419–57, 1995.
- [6] H. C. Barron, R. Auksztulewicz, and K. Friston, “Prediction and memory: A predictive coding account,” *Progress in Neurobiology*, vol. 192, p. 101821, 2020.
- [7] K. L. Stachenfeld, M. M. Botvinick, and S. J. Gershman, “The hippocampus as a predictive map,” *Nature Neuroscience*, vol. 20, no. 11, p. 1643, 2017.
- [8] J. J. Hopfield, “Neural networks and physical systems with emergent collective computational abilities,” *Proceedings of the National Academy of Sciences*, vol. 79, 1982.
- [9] D. Krotov and J. J. Hopfield, “Unsupervised learning by competing hidden units,” *Proceedings of the National Academy of Sciences*, vol. 116, no. 16, pp. 7723–7731, 2019.
- [10] D. Krotov and J. J. Hopfield, “Dense associative memory for pattern recognition,” in *Advances in Neural Information Processing Systems 29: Annual Conference on Neural Information Processing Systems*, 2016.
- [11] A. Radhakrishnan, M. Belkin, and C. Uhler, “Overparameterized neural networks implement associative memory,” *arXiv:1909.12362*, 2019.
- [12] K. Liu, J. Sibille, and G. Dragoi, “Generative predictive codes by multiplexed hippocampal neuronal tupelets,” *Neuron*, vol. 99, no. 6, pp. 1329–1341, 2018.
- [13] J. C. Whittington and R. Bogacz, “An approximation of the error backpropagation algorithm in a predictive coding network with local Hebbian synaptic plasticity,” *Neural Computation*, vol. 29, no. 5, 2017.
- [14] Y. Song, T. Lukasiewicz, Z. Xu, and R. Bogacz, “Can the brain do backpropagation? — Exact implementation of backpropagation in predictive coding networks,” in *Advances in Neural Information Processing Systems 33: Annual Conference on Neural Information Processing Systems*, 2020.
- [15] T. Salvatori, Y. Song, T. Lukasiewicz, Z. Xu, and R. Bogacz, “Predictive coding can do exact backpropagation on convolutional and recurrent neural networks,” *arXiv:2103.03725*, 2021.

- [16] T. Salvatori, Y. Song, T. Lukasiewicz, R. Bogacz, and Z. Xu, “Predictive coding can do exact backpropagation on any neural network,” *arXiv:2103.04689*, 2021.
- [17] D. E. Rumelhart, G. E. Hinton, and R. J. Williams, “Learning representations by back-propagating errors,” *Nature*, vol. 323, no. 6088, pp. 533–536, 1986.
- [18] J. Liu, M. Gong, and H. He, “Deep associative neural network for associative memory based on unsupervised representation learning,” *Neural Networks*, vol. 113, pp. 41–53, 2019.
- [19] T. V. Bliss and T. Lømo, “Long-lasting potentiation of synaptic transmission in the dentate area of the anaesthetized rabbit following stimulation of the perforant path,” *The Journal of Physiology*, vol. 232, no. 2, pp. 331–356, 1973.
- [20] R. C. O’Reilly and J. L. McClelland, “Hippocampal conjunctive encoding, storage, and recall: Avoiding a trade-off,” *Hippocampus*, vol. 4, no. 6, pp. 661–682, 1994.
- [21] K. K. Cowansage, T. Shuman, B. C. Dillingham, A. Chang, P. Golshani, and M. Mayford, “Direct reactivation of a coherent neocortical memory of context,” *Neuron*, vol. 84, no. 2, pp. 432–441, 2014.
- [22] K. Z. Tanaka, A. Pevzner, A. B. Hamidi, Y. Nakazawa, J. Graham, and B. J. Wiltgen, “Cortical representations are reinstated by the hippocampus during memory retrieval,” *Neuron*, vol. 84, no. 2, pp. 347–354, 2014.
- [23] J. J. Hopfield, “Neurons with graded response have collective computational properties like those of two-state neurons,” *Proceedings of the National Academy of Sciences*, vol. 81, 1984.
- [24] K. Steinbuch, “Die Lernmatrix,” *Kybern.*, vol. 1, no. 1, pp. 36–45, 1961.
- [25] M. Demircigil, J. Heusel, M. Löwe, S. Uppang, and F. Vermet, “On a model of associative memory with huge storage capacity,” *Journal of Statistical Physics*, vol. 168, 2017.
- [26] D. Krotov and J. J. Hopfield, “Large associative memory problem in neurobiology and machine learning,” in *International Conference on Learning Representations*, 2021.
- [27] T. Poggio, “From associative memories to powerful machines,” *CBMM Memo No. 114*, 01/2021 2021.
- [28] H. Ramsauer, B. Schäfl, J. Lehner, P. Seidl, M. Widrich, L. Gruber, M. Holzleitner, T. Adler, D. Kreil, M. K. Kopp, G. Klambauer, J. Brandstetter, and S. Hochreiter, “Hopfield networks is all you need,” in *International Conference on Learning Representations*, 2021.
- [29] M. Widrich, B. Schäfl, H. Ramsauer, M. Pavlović, L. Gruber, M. Holzleitner, J. Brandstetter, G. K. Sandve, V. Greiff, S. Hochreiter, *et al.*, “Modern Hopfield networks and attention for immune repertoire classification,” *arXiv:2007.13505*, 2020.
- [30] P. Domingos, “Every model learned by gradient descent is approximately a kernel machine,” *arXiv:2012.00152*, 2020.
- [31] V. Feldman and C. Zhang, “What neural networks memorize and why: Discovering the long tail via influence estimation,” *arXiv:2008.03703*, 2020.
- [32] G. Yang and F. Ding, “Associative memory optimized method on deep neural networks for image classification,” *Information Sciences*, vol. 533, 2020.
- [33] R. Bogacz, “A tutorial on the free-energy framework for modelling perception and learning,” *Journal of Mathematical Psychology*, vol. 76, pp. 198–211, 2017.
- [34] K. Friston, “Learning and inference in the brain,” *Neural Networks*, vol. 16, no. 9, pp. 1325–1352, 2003.
- [35] K. Friston, “A theory of cortical responses,” *Philosophical Transactions of the Royal Society B: Biological Sciences*, vol. 360, no. 1456, 2005.

- [36] J. C. Whittington and R. Bogacz, “Theories of error back-propagation in the brain,” *Trends in Cognitive Sciences*, 2019.
- [37] B. Millidge, A. Tschantz, and C. L. Buckley, “Predictive coding approximates backprop along arbitrary computation graphs,” *arXiv:2006.04182*, 2020.
- [38] A. Ororbia and D. Kifer, “The neural coding framework for learning generative models,” *arXiv:2012.03405*, 2020.

A Detailed derivation of Eqs. (3) and (5)

A.1 Derivation of Eq. (3)

By expanding Eq. (2) with the definition of $\varepsilon_{i,t}^l = x_{i,t}^l - \mu_{i,t}^l$, we have:

$$E_t = \sum_{l=0}^{L-1} \sum_{i=1}^{n^l} \frac{1}{2} (\varepsilon_{i,t}^l)^2 = \sum_{l=0}^{L-1} \sum_{i=1}^{n^l} \frac{1}{2} (x_{i,t}^l - \mu_{i,t}^l)^2. \quad (6)$$

Inference minimizes E_t by modifying $x_{i,t}^l$ proportionally to the gradient of the objective function E_t . We note that each $x_{i,t}^l$ influences E_t in two ways: (i) it occurs in Eq. (6) explicitly, but (ii) it also determines the values of $\mu_{k,t}^{l-1}$ via Eq. (1). Therefore, the derivative of E_t over $x_{i,t}^l$ contains two terms, which are formally as follows:

$$\Delta x_{i,t}^l = -\gamma \cdot \frac{\partial E_t}{\partial x_{i,t}^l} \quad (7)$$

$$= -\gamma \cdot \left(\frac{\partial \frac{1}{2} (x_{i,t}^l - \mu_{i,t}^l)^2}{\partial x_{i,t}^l} + \frac{\partial \sum_{k=1}^{n^{l-1}} \frac{1}{2} (x_{k,t}^{l-1} - \mu_{k,t}^{l-1})^2}{\partial x_{i,t}^l} \right) \quad (8)$$

$$= \gamma \cdot \left(-(x_{i,t}^l - \mu_{i,t}^l) + f'(x_{i,t}^l) \sum_{k=1}^{n^{l-1}} (x_{k,t}^{l-1} - \mu_{k,t}^{l-1}) \theta_{k,i}^l \right) \quad (9)$$

$$= \gamma \cdot \left(-\varepsilon_{i,t}^l + f'(x_{i,t}^l) \sum_{k=1}^{n^{l-1}} \varepsilon_{k,t}^{l-1} \theta_{k,i}^l \right). \quad (10)$$

Considering also the special cases of $l = L$ and $l = 0$, we obtain Eq. (3).

A.2 Derivations of Eq. (5)

The update of weights minimizes E_t by modifying $\theta_{i,j}^{l+1}$ proportionally to the gradient of the objective function E_t . We note that $\theta_{i,j}^{l+1}$ affects the value of the function E_t of Eq. (6) by influencing $\mu_{i,t}^l$ via Eq. (1), hence, the derivative of the objective function E_t over $\theta_{i,j}^{l+1}$ can be formally defined as:

$$\Delta \theta_{i,j}^{l+1} = -\alpha \cdot \partial E_t / \partial \theta_{i,j}^{l+1} \quad (11)$$

$$= -\alpha \cdot \frac{\partial \frac{1}{2} (x_{i,t}^l - \mu_{i,t}^l)^2}{\partial \theta_{i,j}^{l+1}} \quad (12)$$

$$= \alpha \cdot \varepsilon_{i,t}^l f(x_{j,t}^{l+1}). \quad (13)$$

B Further details on the experiments

Here, we provide further details about training PCNs, useful to reproduce them. Particularly, every PCN was trained using IL until convergence, we varied the following hyperparameters and reported the best result: $T \in \{1, 8, 12, 16, 24\}$ for 2-layer networks, and $T \in \{1, 8, 16, 32, 48\}$ for multilayer ones, $\gamma \in \{1, 0.5, 0.1\}$, and $\alpha \in \{0.0001, 0.00005\}$. Furthermore, we have applied a decay factor of 0.9 to γ , applied each time the energy failed to decrease.

We have used standard PyTorch initialization for the weight parameters, and initialized the value nodes to be equal to the value nodes of the previous iteration. We have always performed full batch training, and used ReLU activations in every layer. To retrieve corrupted images, we have iterated the function F 30 times, using $T \in \{100, 250, 500\}$, and reported the best results. To conclude, every image has pixels normalized in $[0, 1]$ by default.

Modern Hopfield networks (MHNs): To perform the experiments on MHNs, we have used the official implementation, provided by the authors and available online. We now provide further details about the experiments, which are sufficient to replicate the results.

For the experiments on MHNs, the parameter β was extensively tested, as we have used $\beta \in \{1, 2, 3, 5, 10, 100, 1000\}$, and always reported the best result. The input images are preprocessed like in all the other experiments of the paper: the images are transformed to PyTorch tensors without further modifications. For experiments comparing against classical Hopfield networks, we have converted every image to binary.

By using the above library and parameters, it is possible to replicate the conducted experiments, as no extra detail/hyperparameter is needed.

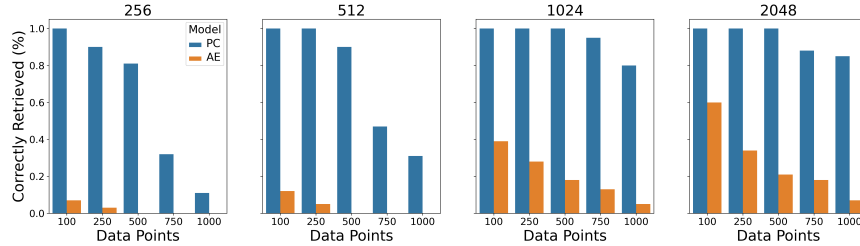


Figure 11: Percentage of correctly retrieved images by 2-layer generative PCNs (PC) and 3-layer autoencoders (AE) with hidden-layer dimensions of 256, 512, 1024, and 2048, when presented with a corrupted image with Gaussian noise of variance 0.2, trained on the Street View House Number dataset.

C Further results with noise of variance 0.2

In this section, we show further results of the experiments in Fig. 4. Particularly, we also include the plots for the Street View House Number dataset, excluded from the paper body due to a lack of space.

Results: The results, plotted in Fig. 11, are similar to the ones of CIFAR10. Again, they show the performance of our method compared to standard autoencoders.

D Analysis of different levels of noise

So far, we analyzed images with Gaussian noise of variance 0.2. We now extend the analysis to different levels of corruptions. Particularly, we have used networks of width $n \in \{512, 1024, 2048\}$ trained on $N \in \{100, 250, 500\}$ natural images taken from the Tiny ImageNet dataset, and tried to retrieve them using Gaussian noise of variance $\eta \in \{0.3, 0.5, 0.7, 1.0\}$.

Results: The results show that our method is able to retrieve stored data points even with a larger amount of variance, although the results get worse the more we increase the level of noise. Particularly, when presented with data points with Gaussian noise with variance 0.3, every network was able to restore at least one image, even when trained on 500 examples. The numbers of retrieved images decreased when increasing the noise. When presented with noise with variance $\eta = 1.0$, only networks with 2048 hidden units were able to retrieve a tiny fraction of the original data points. We report the results in Fig. 12.

E Plots of images with extreme levels of noise

We now plot the images generated using different levels of corruptions. Note that all the images shown here were clearly classified as *not* retrieved by the above analysis. However, we believe that an analysis of not well-retrieved images is still interesting, to understand the limitations of our method. Hence, we trained a generative PCN on 100 images of the Tiny ImageNet dataset, and tried to reconstruct them using extreme levels of noise. Then, we printed the reconstructions.

Results: These representations show that generative PCNs are able to identify the original data points, even if the retrieval process was not accurate enough for the error to fall below the decided threshold 0.005. Particularly, our model was able to identify original memories even when presented with extreme levels of noise ($\eta \in \{1.2, 1.5, 1.7, 2.0\}$), although leaving visible amount of corruption. The reconstructions are given in Fig. 13.

F Analysis of the retrieval function F

Here, we show visually how the function F restores corrupted images. Particularly, we trained a generative PCN with 2048 hidden neurons on 100 images of the Tiny ImageNet dataset, and printed the reconstructions after 1, 6, and 11 iterations of the retrieval function F .

Results: The reconstructions show that the first iteration is able to clear most of the noise. However, further iterations are needed to clear the remaining details, especially if the noise level is high. In fact, it can be observed that one iteration of F is able to retrieve the original data point when the level

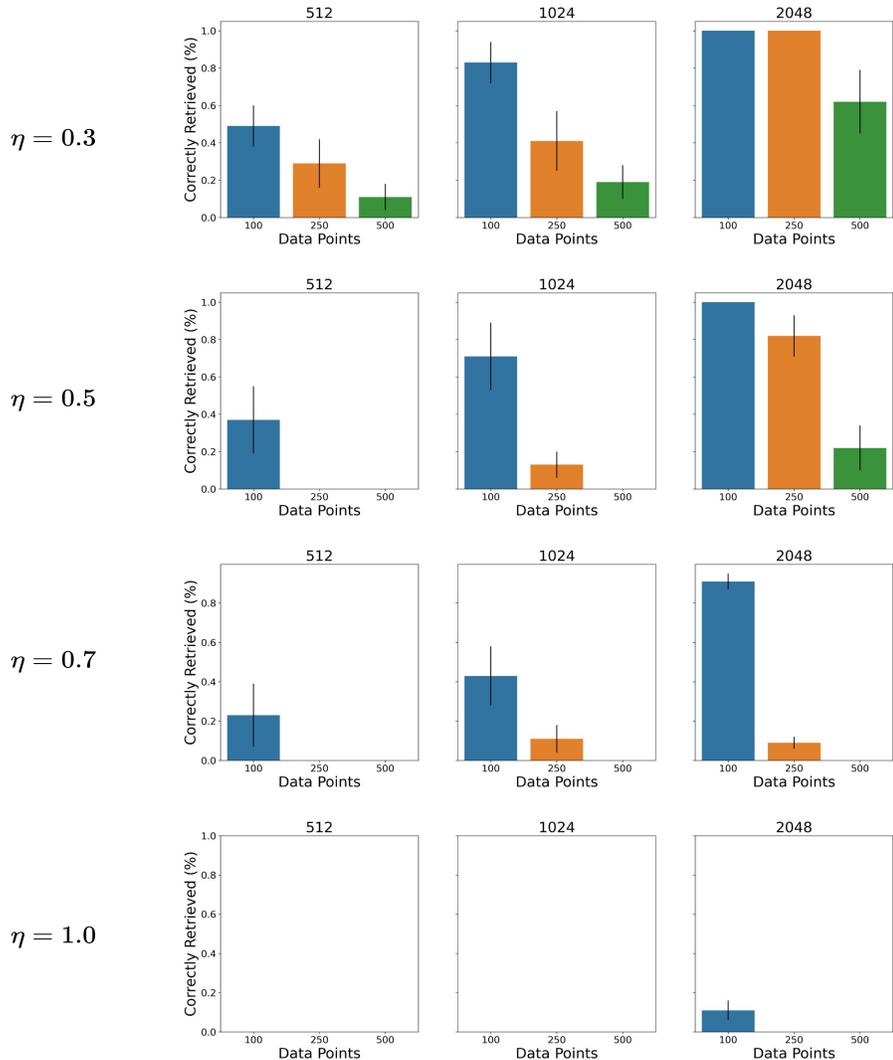


Figure 12: Percentage of correctly retrieved images by 2-layer generative PCNs (PC) with hidden-layer dimensions of 512, 1024, and 2048, when presented with a corrupted image with Gaussian noise of different variances, trained on the Tiny ImageNet dataset.

of corruption is $\eta = 0.3$, but fails when $\eta = 1.0$. This process usually converges around $m = 15$, depending on the number of iterations T and the level of noise. The results are shown in Fig. 14.

G Reconstruction of partial images

To further show the robustness of our experiments, we replicate the experiments of Section 5.1 on the CIFAR10 dataset, training networks of different depths ($L \in \{5, 7, 10\}$) to generate 500 images, and report the results in Fig. 15. Again, we consider a data point to be perfectly reconstructed if the error between the original image and the reconstruction is below 0.001.

Results: The plots confirm the results stated in the body of this work: the deeper the network, the more images are perfectly reconstructed.

H Full-page reconstructions of ImageNet

To show the reconstruction capabilities of our method, in what follows we plot full-page reconstructions of ImageNet pictures.

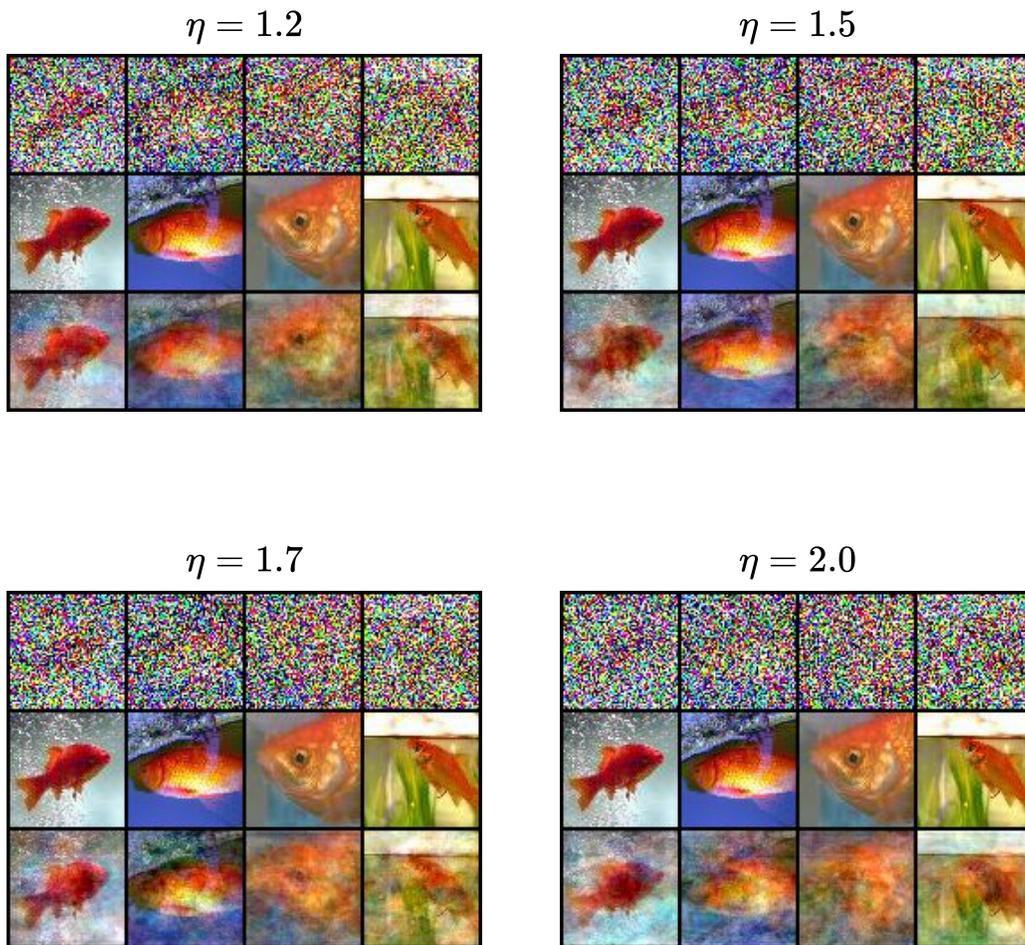


Figure 13: Analysis of the reconstruction capabilities of generative PCNs under different levels of noise $\eta \in \{1.2, 1.5, 1.7, 2.0\}$. Every plot was obtained using a 2-layer generative PCN with 2048 hidden units, trained on 100 images of the Tiny ImageNet dataset.

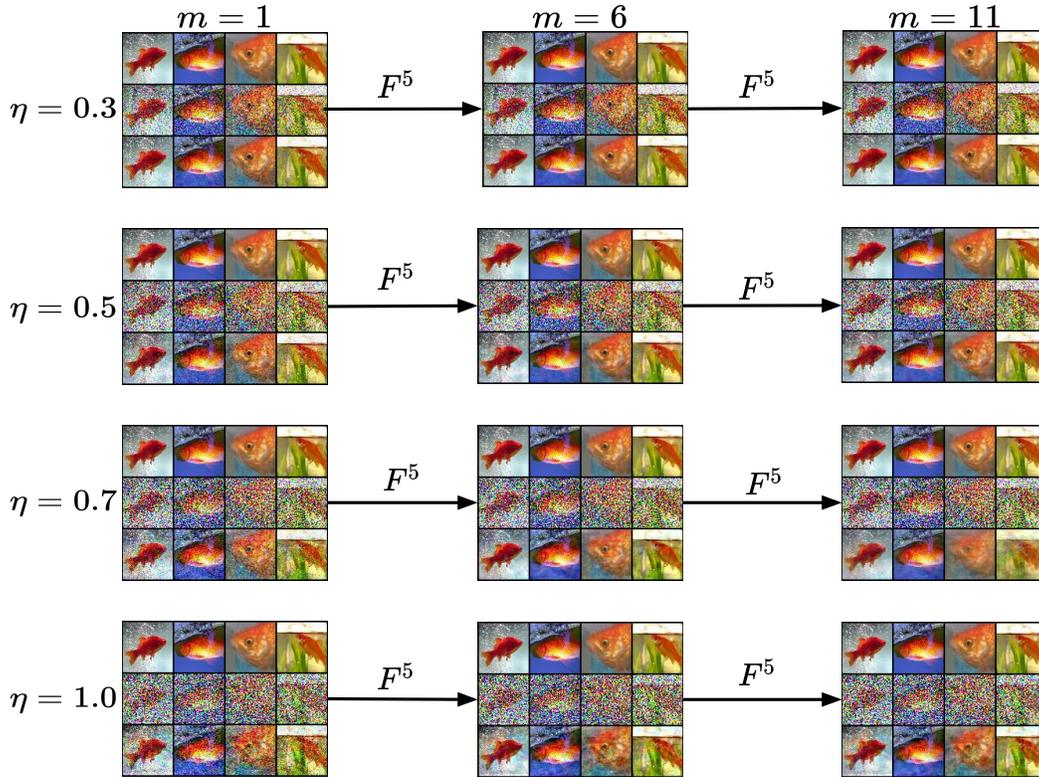


Figure 14: Analysis of the reconstruction capabilities of 10 iterations of the function F under different levels of noise $\eta \in \{0.3, 0.5, 0.7, 1.0\}$. Particularly, we plotted the results after 1, 6, and 11 iterations of F .

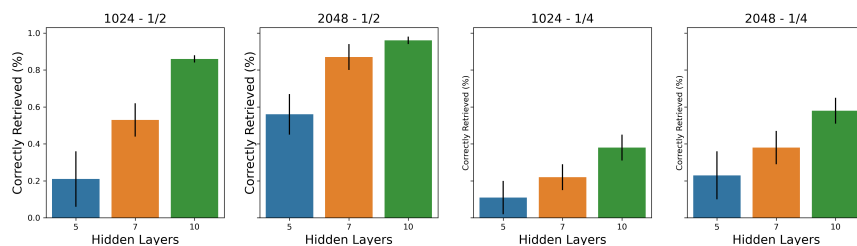


Figure 15: Percentage of correctly retrieved images as a function of the number of hidden layers, for generative PCNs on a dataset of 500 images of the CIFAR10 dataset. We used networks with $n = \{1024, 2048\}$ hidden neurons, and tried to reconstruct them using partial images containing a fraction of $1/2$ and $1/4$ of the original images.

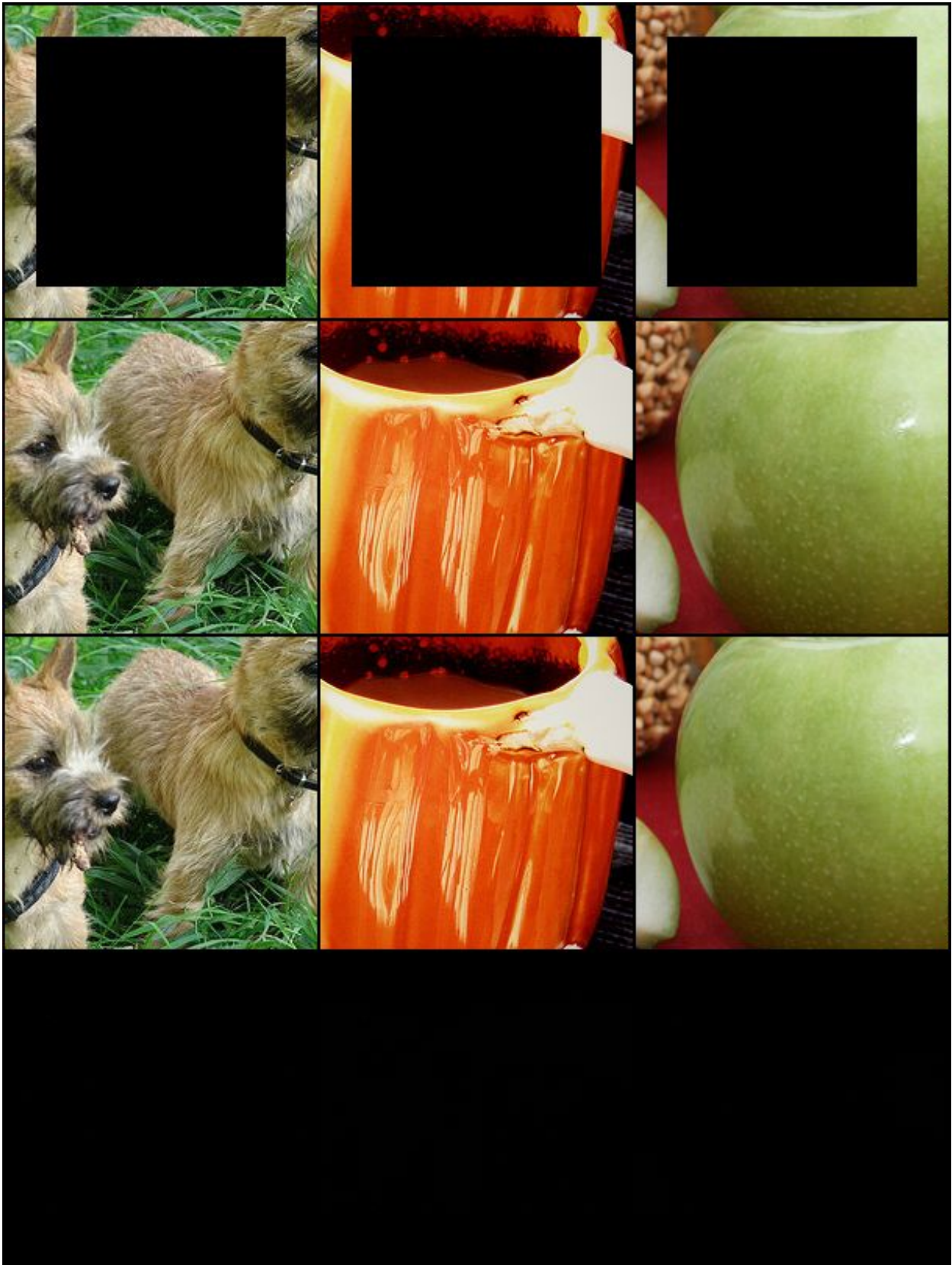


Figure 16: To show the level of accuracy of our proposed method, we represent reconstructions of ImageNet images. Here, a reconstruction when a patched image is presented to our generative PCN. From top to bottom: partial image, reconstructed image, original image, and reconstruction error (difference between original and reconstruction).

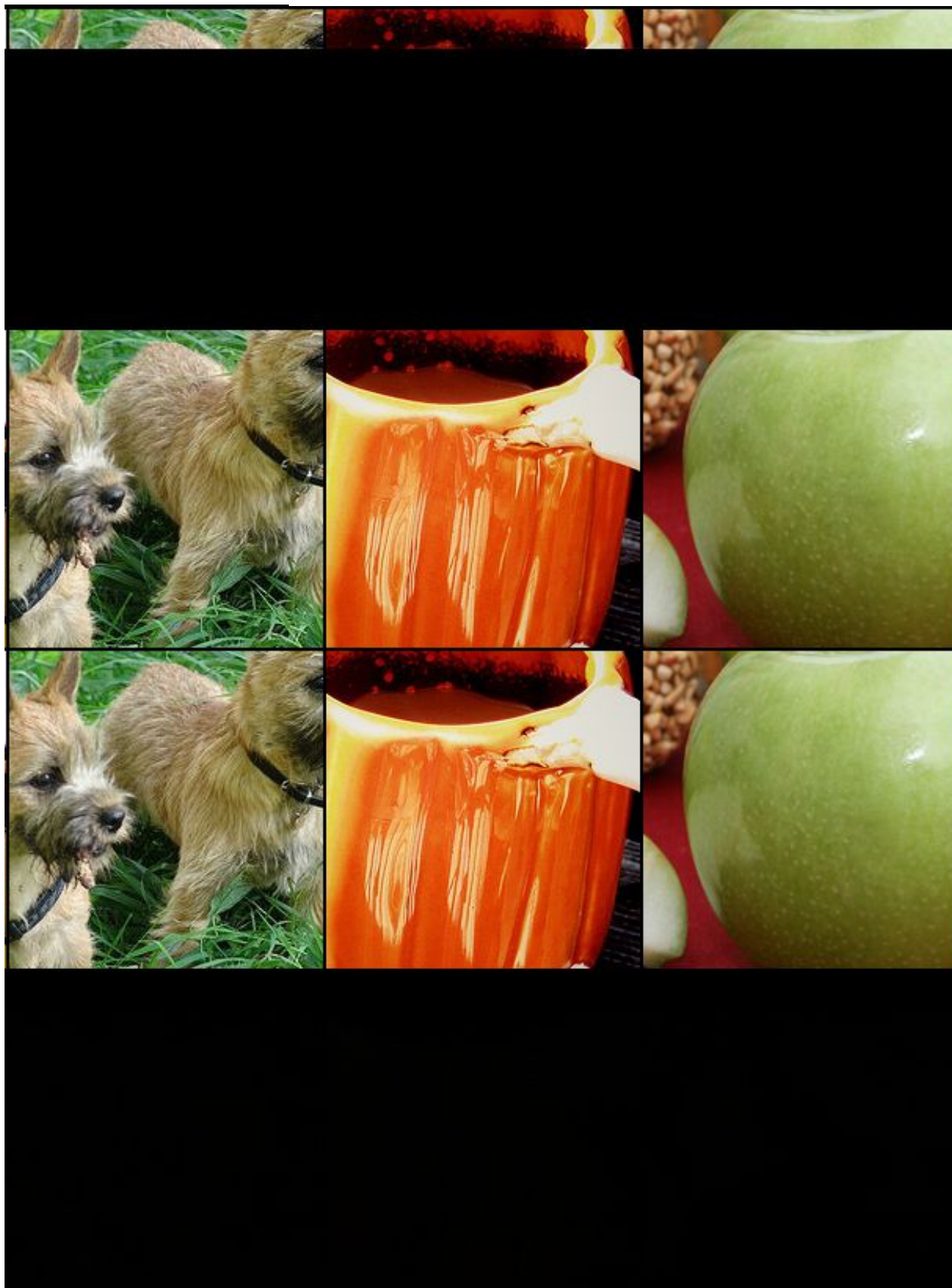


Figure 17: To show the level of accuracy of our proposed method, we represent reconstructions of ImageNet images. Here, a reconstruction when only $1/8$ of the original picture is presented to our generative PCN. From top to bottom: partial image, reconstructed image, original image, and reconstruction error (difference between original and reconstruction).